JOURNAL OF VIROLOGY, Apr. 2004, p. 3361–3371 Vol. 78, No. 7
0022-538X/04/$08.00+0 DOI: 10.1128/JVI.78.7.3361–3371.2004

Structure of Adeno-Associated Virus Serotype 5

Robert W. Walters,[1,2]† Mavis Agbandje-McKenna,[3]† Valorie D. Bowman,[4]† Thomas O. Moninger,[1] Norman H. Olson,[4] Michael Seiler,[1] John A. Chiorini,[5] Timothy S. Baker,[4] and Joseph Zabner[1]*

Departments of Internal Medicine[1] and Physiology and Biophysics,[2] College of Medicine, University of Iowa, Iowa City, Iowa 52242; Department of Biochemistry and Molecular Biology, Center for Structural Biology, The Brain Institute, University of Florida College of Medicine, Gainesville, Florida 32610[3]; Department of Biological Sciences, Purdue University, West Lafayette, Indiana 47907[4]; and Gene Therapeutics Branch, National Institute of Dental and Craniofacial Research, National Institutes of Health, Bethesda, Maryland 20892[5]

Received 2 September 2003/Accepted 4 December 2003

Adeno-associated virus serotype 5 (AAV5) requires sialic acid on host cells to bind and infect. Other parvoviruses, including Aleutian mink disease parvovirus (ADV), canine parvovirus (CPV), minute virus of mice, and bovine parvovirus, also bind sialic acid. Hence, structural homology may explain this functional homology. The amino acids required for CPV sialic acid binding map to a site at the icosahedral twofold axes of the capsid. In contrast to AAV5, AAV2 does not bind sialic acid, but rather binds heparan sulfate proteoglycans at its threefold axes of symmetry. To explore the structure-function relationships among parvoviruses with respect to cell receptor attachment, we determined the structure of AAV5 by cryo-electron microscopy (cryo-EM) and image reconstruction at a resolution of 16 Å. Surface features common to some parvoviruses, namely depressions encircling the fivefold axes and protrusions at or surrounding the threefold axes, are preserved in the AAV5 capsid. However, even though there were some similarities, a comparison of the AAV5 structure with those of ADV and CPV failed to reveal a feature which could account for the sialic acid binding phenotype common to all three viruses. In contrast, the overall surface topologies of AAV5 and AAV2 are similar. A pseudo-atomic model generated for AAV5 based on the crystal structure of AAV2 and constrained by the AAV5 cryo-EM envelope revealed differences only in surface loop regions. Surprisingly, the surface topologies of AAV5 and AAV2 are remarkably similar to that of ADV despite only exhibiting ~20% identity in amino acid sequences. Thus, capsid surface features are shared among parvoviruses and may not be unique to their replication phenotypes, i.e., whether they require a helper or are autonomous. Furthermore, specific surface features alone do not explain the variability in carbohydrate requirements for host cell receptor interactions among parvoviruses.

Recombinant adeno-associated viruses (AAV) hold promise for gene transfer to several tissues (14–16, 27, 30, 32, 38). These viruses belong to the *Dependovirus* genus of the single-stranded-DNA virus family *Parvoviridae*, requiring helper functions from either herpesvirus or adenovirus for replication. They are nontoxic and have not been linked to any disease. AAV capsids contain 60 protein subunits and include a combination of three proteins, VP1, VP2, and VP3, which are encoded by the same RNA message but are the products of alternative splicing. The structure of the parvovirus capsid protein (VP2 or VP3, depending on the virus) includes a highly conserved β-barrel motif, which forms the core contiguous capsid in all of the structures, and loop insertions between the β-strands, which form a varied surface topology (2). AAV type 2 (AAV2) was the first primate AAV to be cloned into a plasmid, and it has been studied extensively (37). AAV2-based vectors have been used to mediate factor IX gene transfer to human muscles, making hemophilia one of the first genetic diseases to be partially corrected by gene transfer (27). AAV2 has also been investigated in vitro and in vivo for use in gene transfer of the cystic fibrosis transmembrane conductance regulator cDNA to airway epithelia for cystic fibrosis treatment (6, 13, 15, 16, 39, 45). However, because AAV2 is inefficient at transducing airway epithelia, as well as other cell types (e.g., brain neurons and retina photoreceptors), additional serotypes have been investigated (24, 50, 52).

We found that a divergent AAV serotype, AAV5, binds and infects from the apical surface of human airway epithelia more efficiently than AAV2 (52). Moreover, AAV5 requires sialic acid for binding and infection (26, 46) rather than the heparan sulfate proteoglycan used by AAV2. Mutational analysis (33, 48) and the recently published X-ray crystal structure of AAV2 (49) indicated that several basic residues of AAV2 control heparan binding. These residues cluster on the inner surfaces of the protrusions around the threefold axes. In contrast, the AAV5 residues required for sialic acid binding have not been identified. Hence, while transduction studies indicated that AAV5 can expand the utility of AAV viruses for gene transfer, further investigations are necessary to help exploit the full potential of AAV5 as a vector.

Interestingly, a number of autonomously replicating parvoviruses also bind sialic acid, suggesting a structural homology beyond that expected of viruses in the same family. Aleutian mink disease parvovirus (ADV), bovine parvovirus, and minute virus of mice (MVM) bind sialic acid, and infection by them can be inhibited by pretreatment of target cells with neuraminidase (12, 17, 40). However, the exact amino acids that bind sialic acid are not known. In contrast, canine parvovirus (CPV) binds sialic acid, but this activity is not required

* Corresponding author. Mailing address: University of Iowa College of Medicine, 500 EMRB, Iowa City, IA 52242. Phone: (319) 353-5511. Fax: (319) 335-7623. E-mail: joseph-zabner@uiowa.edu.

† R.W.W., M.A.-M., and V.D.B. contributed equally to this work.

for infectivity (5, 42). Rather, CPV infects cells by binding canine transferrin receptor (34). The residues required for canine transferrin receptor binding are still under investigation (23). The CPV capsid sequence determinants of sialic acid binding line the walls of the depressions at the icosahedral twofold axes (42). All known parvovirus structures have depressions at the icosahedral twofold axes. Thus, these features of CPV may help us to determine the sialic acid binding motif of AAV5.

Cryo-electron microscopy (cryo-EM) studies have demonstrated that ADV possesses features that distinguish it from other autonomous parvoviruses (31). In particular, three prominent, mound-like protrusions (referred to as mounds from here on) decorate the ADV surface near each threefold axis of symmetry, whereas in CPV and MVM, a pinwheel-like structure arises from intertwined, symmetry-related surface loops (3, 43). A pseudo-atomic model of the ADV capsid suggested that the ADV mounds also include a clustering of symmetry-related surface loops (31). However, the limited resolution (22 Å) of the cryo-EM density map of ADV precluded a precise residue assignment. Notably, recent cryo-EM and X-ray structures of AAV2 also showed three mounds rather than a pinwheel (29, 49). However, the ADV mounds are larger than those in AAV2 because ADV contains additional amino acids in the loops that form this structure (31). This sequence is absent from all other parvoviruses.

The diameters of the depressions at the icosahedral twofold axes of parvovirus capsids also differ (31). The depression is much wider in CPV than in ADV, MVM, and AAV2 (3, 29, 31, 49). Hence, though parvovirus capsids share structural homology, some regions, particularly those on the capsid surface, vary. Notable differences include narrow versus wide depressions at the twofold axes and three mounds versus a pinwheel-like structure at the threefold axes. Conserved features include a canyon-like depression that encircles protrusions of varied shapes at the fivefold axes (43).

Structural studies have provided valuable insights into the functional properties of parvovirus capsids (10, 29, 31, 47). An analysis of parvovirus capsids has also shown that surface variations correlate with phenotypic differences, such as cell surface recognition and antigenicity, both of which are conferred by different sets of surface residues (1). In this study, we used both cryo-EM and homology-based modeling to probe the capsid structure of AAV5. The pseudo-atomic model generated for AAV5, constrained by its reconstructed cryo-EM envelope, provided a means for predicting possible sialic acid binding regions on the capsid, based on the CPV sialic acid binding data. In addition, this model was compared to the available AAV2 capsid structure to further probe structural differences among AAV serotypes that specify tissue tropism and antigenicity.

MATERIALS AND METHODS

Propagation and purification of AAV5. Wild-type AAV5 was produced by coinfecting COS cells with wild-type AAV5 and wild-type adenovirus. Prior to their use, COS cells and seed stocks of wild-type adenovirus were screened by PCR for wild-type AAV contamination. COS cells grown to 50% confluence were infected for 1 h at 37°C with 1 multiplicity of infection (MOI) of wild-type AAV5 and 1 MOI of wild-type adenovirus delivered in Eagle's minimal essential medium. Serum-containing medium was then added, and the cells were cultured for an additional 72 h.

At 72 h postinfection, cells were harvested by scraping and pelleted by low-speed centrifugation. For every 10 plates, the pellet was resuspended in 5 ml of tissue dissociation buffer (140 mM NaCl, 5 mM KCl, 0.7 mM K_2HPO_4, 25 mM Tris-HCl, pH 7.4) and stored at −70°C. The cell pellet was thawed at 37°C, and benzonase (Sigma Chemical Co.) was added to a final concentration of 20 U/ml. Sodium deoxycholate was then added to a final concentration of 0.5%, and the suspension was incubated for 1 h. The suspension was homogenized thoroughly (20 strokes in a Wheaton B homogenizer). Next, CsCl was added to a final density of 1.4 g/cm^3, and the homogenate was centrifuged in polyallomer tubes in an SW40 rotor at 38,000 rpm for 65 h at 20°C. The gradients were fractionated by side puncture. Fractions with a refractive index of 1.373 to 1.371 were pooled, centrifuged in an SW50.1 rotor, and fractionated as described above. A third round of centrifugation was completed in the same manner as the second round. Refractive indices were determined by using a refractometer (Fisher Scientific).

AAV5 viruses were titrated by Southern blotting and transmission EM. The virus titers for wild-type preparations reached 5×10^{14}/ml. The viruses were screened for wild-type adenovirus by a serial dilution assay using a fluorescein isothiocyanate-hexon antibody (sensitivity, 1 particle in 10^5) (53).

Cryo-EM and three-dimensional image reconstruction. Small aliquots (3 μl) of AAV5 samples were placed on carbon-coated copper grids, blotted with filter paper, and plunged into a liquid ethane slush to suspend the particles in a thin layer of vitreous ice, as described previously (4). The grids were inserted into a precooled Gatan 626 cryotransfer holder (Gatan Inc., Warrendale, Pa.) that maintained a constant temperature of −176°C. Frozen-hydrated AAV5 samples were examined with a CM200 FEG transmission electron microscope (Philips Electronic Instruments, Mahwah, N.J.), and images were recorded onto Kodak SO-163 film. A low-magnification (×4,560) survey image was captured with a 2K by 2K pixel slow-scan charge-coupled device camera, and candidate areas for high-magnification imaging were identified prior to photography. Images of individual, empty capsids were then recorded at 200 kV at a magnification of ×38,000, with underfocus values ranging from 0.7 to 3.5 μm, with a dose of ~14.5 $e^-/Å^2$/image. The initial orientation and origin parameters of the images for the reconstruction were determined by a model-based refinement approach (4) that used the three-dimensional reconstruction of ADV (31) as the initial model. The orientation and origin parameters for each particle were refined in an iterative procedure that used the most current AAV5 reconstruction as a model for the subsequent refinement cycle. Of the 1,552 individual, empty particle images selected from the digitized micrographs, 695 were used to compute a final three-dimensional reconstruction to 16-Å resolution. The resolution was estimated according to established procedures (4). All calculated eigen values exceeded 10.0, which indicated that random and unique data were used for each reconstruction.

Alignment and modeling. A pseudo-atomic model of the AAV5 VP3 capsid protein was built by threading its amino acid sequence through the backbone of the known atomic structure of CPV, based on a sequence alignment generated by Clustal W (v. 1.4) (41). Each differing amino acid was interactively mutated from that of CPV to that of AAV5 by the program O (25, 28). Residues were deleted or added from the O database to account for gaps in the alignment. Due to the relatively low resolution of the map (16 Å), it was not possible to adjust the side chains of residues that differed between AAV5 and CPV or those that were inserted from the database. The main chain of a single AAV5 VP3 model, in a standard icosahedral orientation, was fit into the reconstruction density as a rigid body. Several surface loops in the model had to be adjusted from their positions in CPV to fit the reconstruction density of the AAV5 capsid. The adjusted model was subjected to energy minimization by CNS software (9). After refinement, the 60 proteins that make up the complete particle were generated by geometrical transformations which applied icosahedral symmetry operators to the single VP3 model. The main chain atoms for the complete particle were used to compute an electron density map for comparison with the original cryo-EM density map, using the overlap map subroutine in CCP4 (11), which compares equivalent sections.

A pseudo-atomic model of the AAV5 VP3 capsid protein based on AAV2 was built by use of SwissModel, which uses the program O (20, 35, 36). The primary sequence of AAV5 VP3 was submitted to SwissModel along with the known structure of AAV2 as a template (1LPA) (49). Due to the resolution of the reconstruction, only main chain atoms of the VP3 molecule, in a standard icosahedral orientation, were fit into the map as a rigid body. The 60 proteins that make up the complete particle were generated by matrix multiplication using icosahedral symmetry operators. Only one adjustment of the model was required. This involved moving a surface loop (residues 253 to 259) into the density from its position outside the reconstruction envelope. The pseudo-atomic capsid model was also used to generate an electron density map of equivalent resolution and grid size to the those of the original cryo-EM map for comparison, using the overlap map subroutine in

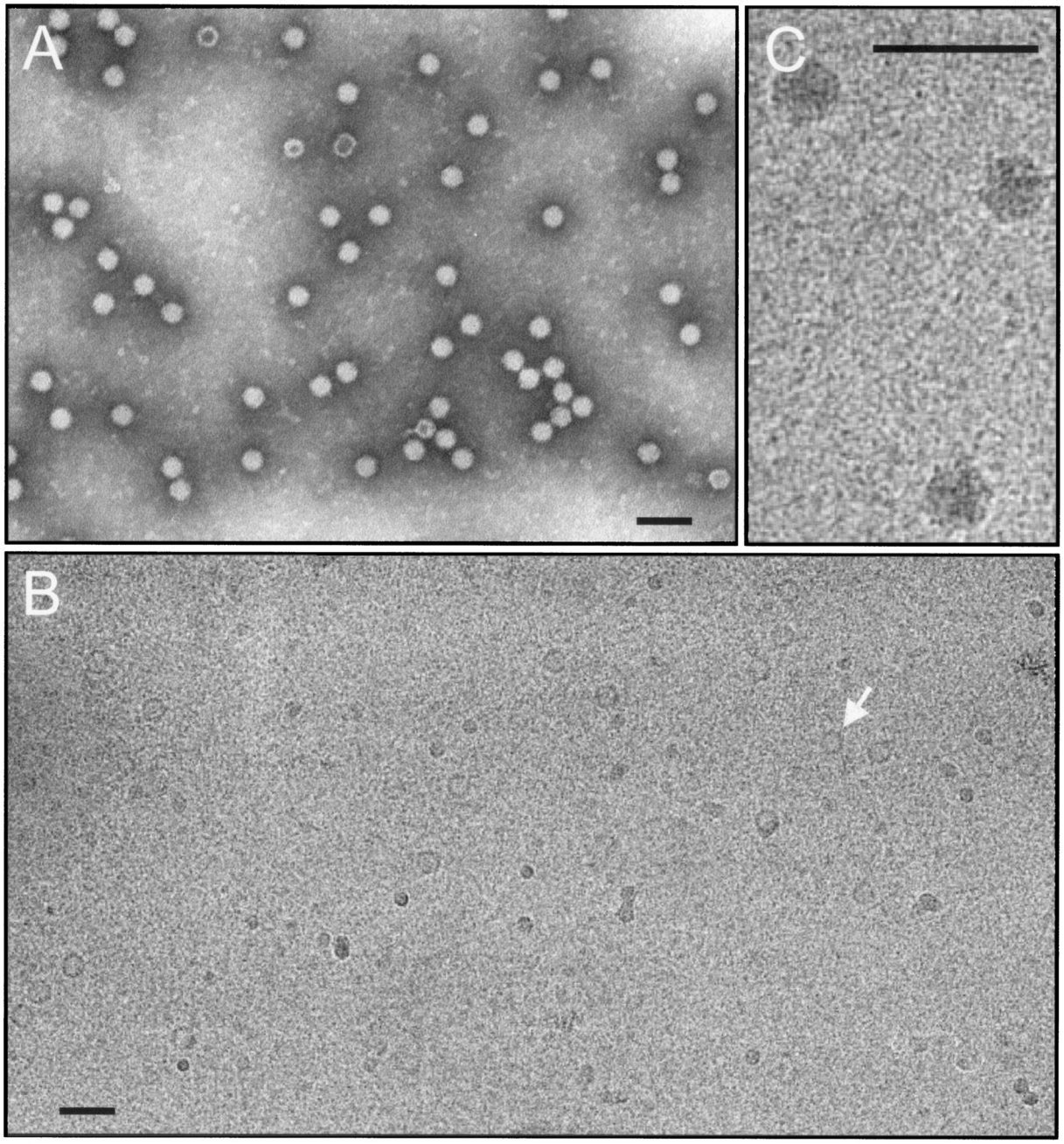

FIG. 1. Electron photomicrographs of AAV5. (A) Transmission electron micrograph of negatively stained virus. (B) Low-magnification view of AAV5 suspended in a layer of vitreous ice. The arrow indicates a viral particle. (C) High-magnification view of AAV5 in vitreous ice. Bars, 50 nm.

CCP4 (11). For the prediction of possible sialic acid binding residues of AAV5, a least-squares superposition of the AAV2-based model of AAV5 on the capsid structure of CPV was performed with the program O (25, 28).

RESULTS

Capsid structure of AAV5. The structure of AAV5 was determined by means of well-established cryo-EM and three-dimensional image reconstruction methods (4). The integrity of AAV5 particles was checked by the examination of negatively stained viral samples by transmission EM (Fig. 1A). Micrographs of unstained, vitrified AAV5 particles, which exhibit less contrast than those that were stained (Fig. 1B and C), were used to compute a three-dimensional image reconstruction of AAV5 to 16-Å resolution (Fig. 2). The capsid structure had mean external radii of 120, 131, and 127 Å at the icosahedral twofold, threefold, and fivefold axes of symmetry, respectively (Fig. 2). Characteristic features of the AAV5 capsid include a depression at each twofold axis (Fig. 2B), three mounds adjacent to each threefold axis (Fig. 2C), and a shallow depression that encircles a dimpled, pentameric protrusion at each fivefold axis (Fig. 2D).

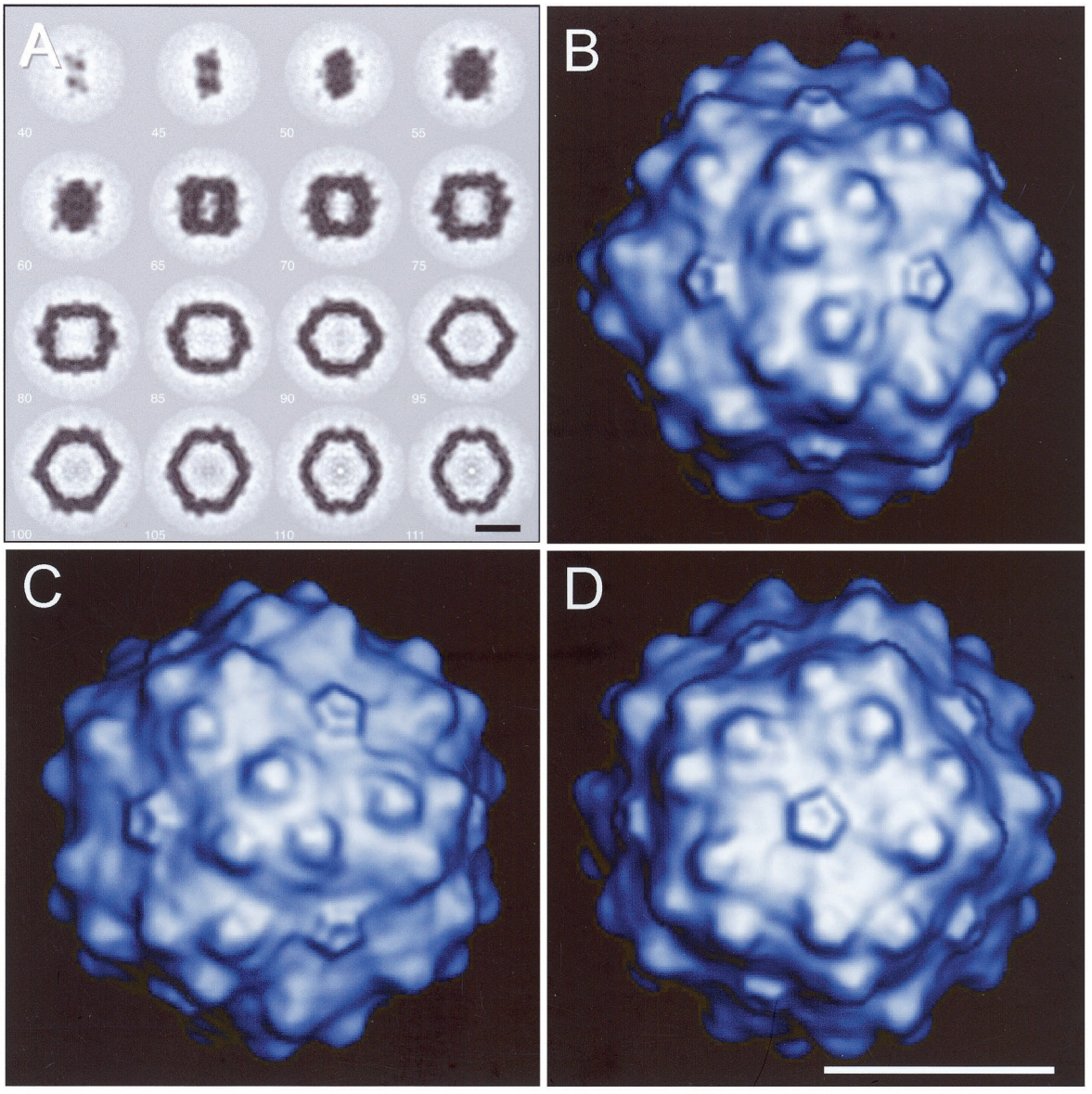

FIG. 2. Three-dimensional reconstruction of AAV5. (A) Sequential sections of the capsid viewed down the twofold axis of icosahedral symmetry. Also shown are shaded surface representations of the reconstruction viewed down a twofold (B), threefold (C), and fivefold (D) axis. The reconstruction was computed to 16 Å from images of 695 different AAV5 particles. Bar, 10 nm.

Comparison of AAV5 surface topology with those of other parvoviruses. As a means to explore similarities and differences between AAV5 and available autonomous parvovirus structures known to bind sialic acid, we compared the capsid structures of ADV, CPV, and AAV5. Within this virus family, ADV and CPV provide representative examples of capsids with distinct surface topologies (i.e., wide versus narrow depressions at the twofold axes and three mounds versus a pinwheel at or surrounding the threefold axes). The high-resolution X-ray crystal structure of CPV was band-pass filtered to produce a low-resolution structure for direct comparison with the ADV and AAV5 image reconstructions (Fig. 3). CPV has a large, open depression at each twofold axis, whereas ADV has small, narrow depressions and AAV5 has no depressions at these positions (Fig. 3). Three similarly oriented mounds surround each threefold axis in ADV and AAV5. This contrasts with the pinwheel-like feature at each threefold axis in CPV. Notably, the protrusions in ADV are more prominent than in AAV5, presumably because the VP2 protein of ADV contains additional residues (31). ADV and CPV both have deep canyons with steep walls surrounding each fivefold axis, whereas the corresponding surface of AAV5 is relatively smooth and featureless. CPV and AAV5 both have dimpled mounds of density at each fivefold axis, although in CPV it is broad and conical, with a large dimple, and in AAV5 it is small and pentagonal and the dimple is correspondingly small as well as shallow. ADV has a mound-like protrusion at each fivefold axis that appears quite similar to the mounds near the threefold

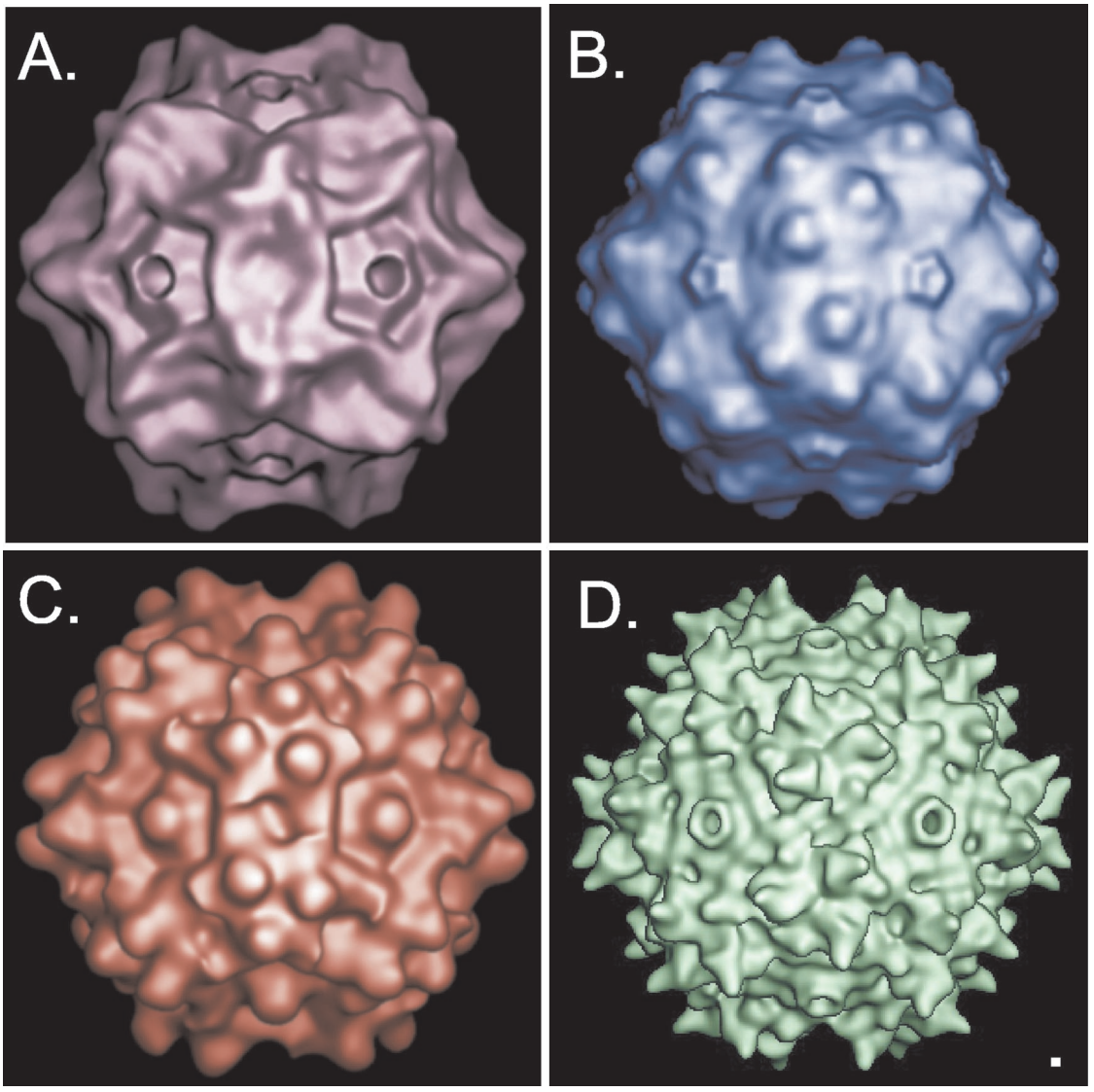

FIG. 3. Comparison of AAV5 structure with AAV2, CPV, and ADV structures. Shaded surface representations of CPV (A), AAV5 (B), ADV (C), and AAV2 (D), all viewed down a twofold axis of symmetry, are shown. The atomic structures of the CPV capsid (43) and AAV2 were rendered to a 21-Å resolution. The three-dimensional cryo-EM reconstruction of ADV capsids (31) is shown at a 22-Å resolution.

axes. Thus, the surfaces of AAV5, CPV, and ADV share some, but not all, characteristic features, and no single feature is common to all three viruses.

The capsid structure of AAV5 was also compared to that of AAV2, the only other dependovirus for which a near-atomic-resolution three-dimensional structure is available (49). When AAV2 was rendered at a 21-Å resolution, its surface topology closely corresponded to that of the observed envelope of the AAV5 cryo-EM reconstruction (Fig. 3D). This is consistent with results obtained for other parvoviruses with 50% or more amino acid sequence identities (3). Despite widespread similarities between AAV2 and AAV5, the most notable difference occurs in the threefold axis-related mounds, which are larger and more pointed in AAV2 than in AAV5 (29). Hence, though AAV2 and AAV5 differ in their binding properties, their capsid morphologies are remarkably similar.

Model-based comparison of AAV5 and CPV. To help predict the location of the sialic acid binding site on AAV5, we generated a pseudo-atomic homology model of AAV5 based on an alignment of the VP3 sequences for CPV and AAV5. This alignment revealed regions of high conservation in the core β-strands and within the N and C termini. These conserved regions were interspersed by highly variable sequences which formed surface loops (Fig. 4A; also data not shown). A comparison of the backbone topology of the AAV5 homology model (cyan) with that of CPV (red) showed that the core β-strand structure of AAV5 resembles that of CPV (Fig. 4A, lower left portion). Conversely, the remaining portions of the AAV5 model exhibited almost no similarity to the CPV template (Fig. 4A, top and right portions). These observations are consistent with the global comparison of CPV and AAV5 surface topologies (Fig. 3) described above and with the results of

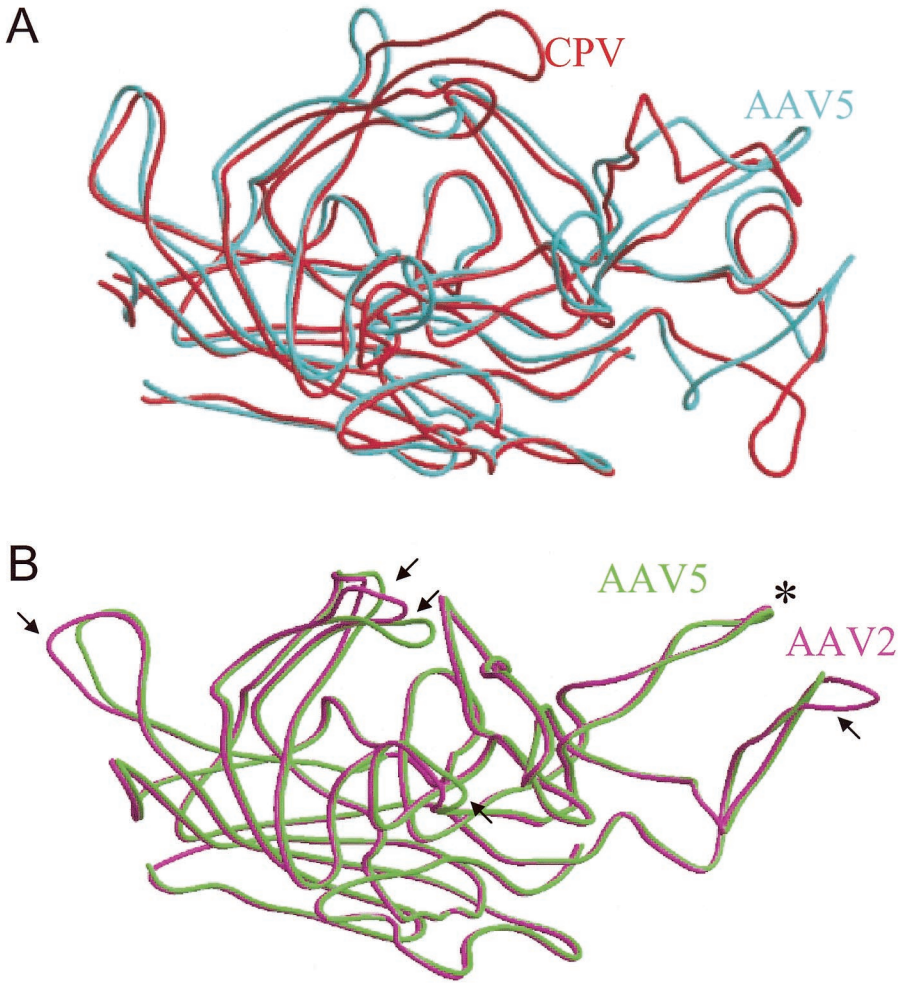

FIG. 4. Modeling of AAV5 based on CPV and AAV2 crystal structures. (A) Homology model of AAV5 (cyan) based on the CPV crystal structure superimposed on the CPV structure (red). (B) Homology model of AAV5 (green) based on the AAV2 crystal structure superimposed on the AAV2 structure (magenta). Differences between the AAV2-based model of AAV5 and AAV2 occur in the surface loops marked by arrows. The asterisk identifies the heparan binding loop in AAV2.

sequence alignment (data not shown). Since variable regions account for the surface topologies of parvovirus capsids, which determine phenotypes, it remains to be seen if CPV constitutes a suitable model for investigation of the molecular determinants of AAV5 receptor recognition by mutational analysis.

Model-based comparison of AAV5 and AAV2. Given the significant differences in the surface properties of AAV5 and CPV, we next compared our AAV5 model to the high-resolution structure of AAV2 (49), with which it shares significant sequence identity (Fig. 5). As predicted, the highly conserved core β-barrel and N and C termini were interspersed with variable regions (Fig. 5). The AAV2 structure was then used as a template to generate a second homology model of AAV5 (green) which was strikingly similar to that of AAV2 (magenta) (Fig. 4B). Differences between these structures are confined to four short loops in which the highest sequence variability among AAV serotypes occurs (18).

The accuracy of the AAV2-based model of AAV5 was checked by the generation of 60 copies of the VP3 protein and their placement into the cryo-EM density by a rigid body protocol (Fig. 6A). In addition, we calculated structure factors from the model and generated an electron density map at 16-Å resolution by use of CCP4 (11) for comparison with the cryo-EM reconstruction (Fig. 6B). This map correlated quite well with the original reconstructed density (Fig. 6A). Based on this close correspondence, we adopted the AAV2-based model of AAV5 as our working model.

Focusing on the mounds at the threefold axes, the AAV5 model (green) fit the AAV5 capsid reconstruction quite well (Fig. 6C). Only one adjustment of the model was required to maximize the quality of the fit. A divergent surface loop (residues 253 to 259) was folded down to best fit the reconstruction density. For comparison, we also superimposed the AAV2 template (magenta) with the AAV5 model and found that two loops protruded outside the AAV5 reconstruction envelope (Fig. 6C, arrows X and Y). AAV2 loop X (residues 263 to 268) is the equivalent of the AAV5 divergent loop (residues 253 to 259) mentioned above. AAV2 loop Y contains six residues (positions 451 to 457) that are missing from AAV5 (Fig. 5). This loop lies next to the heparan sulfate binding loop of

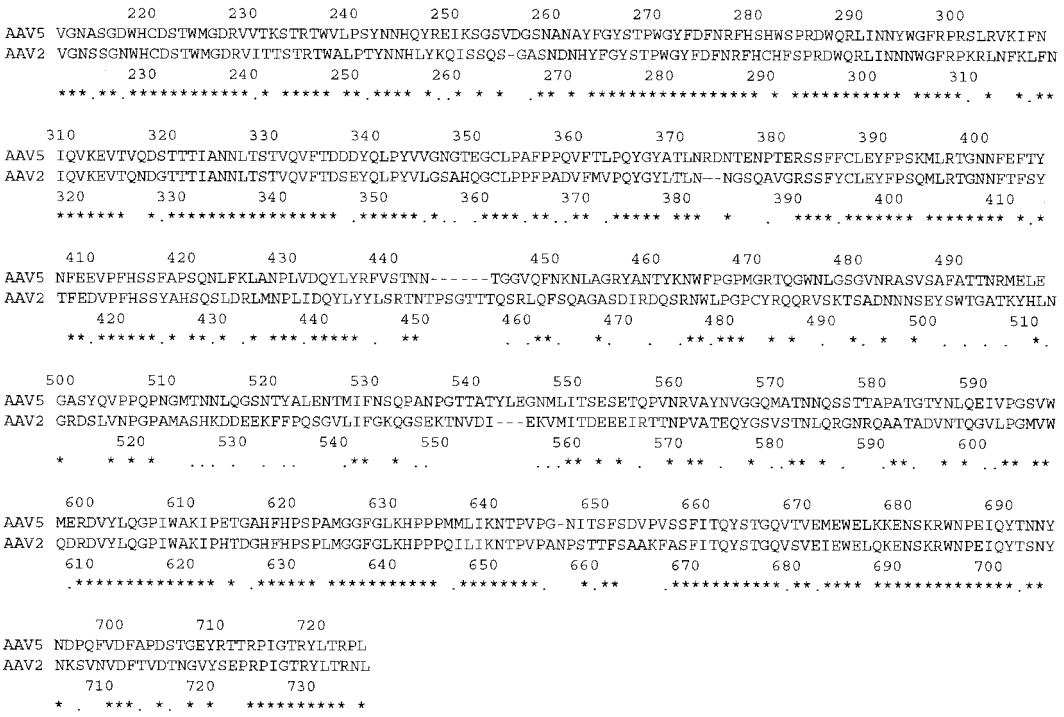

FIG. 5. Sequence alignment of AAV5 and AAV2. Asterisks indicate amino acid identities, and dots indicate conserved residues.

AAV2 (Fig. 4B, asterisk). Hence, loop Y may play a role in the heparan sulfate binding site, and we suggest that its absence from AAV5 may explain why AAV5 does not bind heparan sulfate. All of the differences between AAV2 and the AAV5 model reside on the capsid surface, which likely explains their differences in tissue tropism and antigenic phenotypes. Although there are key differences between AAV2 and the AAV5 model, the AAV2-based model should prove useful for sequence-based studies of AAV5 and perhaps of other AAV serotypes as well.

Model-based predictions of AAV5 sialic acid binding residues. Comparisons of the ADV, CPV, and AAV5 capsids, all of which are known to bind sialic acid, suggested that no single surface feature correlates with this phenotype. Hence, we superimposed our working model of AAV5 onto the capsid structure of CPV to help predict which residues of AAV5 may bind sialic acid. An asparagine (N396) and two arginines (R377 and R397) are part of the wall in the depression at the icosahedral twofold axis in CPV and mediate sialic acid binding (42). A short segment of the AAV2-based model of AAV5 superimposed on the CPV structure illustrates the spatial relationship between the CPV sialic acid binding residues and the analogous region of the AAV5 model (Fig. 7A). Two of the spatially equivalent AAV5 residues (N546 and M547) also cluster on the capsid surface on the wall of the twofold depression, while the third (I528) is slightly buried (Fig. 7B). To our knowledge, there are no consensus motifs described for sialic acid binding, although structural studies of protein-carbohydrate complexes suggest the participation of acidic residues as favoring these types of interactions (M. Agbandje-McKenna, unpublished observations).

DISCUSSION

The ability to engineer viral vectors with an altered tropism raises the hope that tissue-specific gene transfer vectors can be produced in sufficient quantities for therapy. Recently, progress was made in the retargeting of adenovirus vectors. This was facilitated by a structure-based analysis of the interactions of the attachment protein-receptor complex (i.e., adenovirus fiber knob bound to the coxsackievirus-adenovirus receptor [CAR]) (7). Based on these data, adenoviruses have been designed that do not bind to CAR but are retargeted to other specific receptors. Hence, in a similar vein, understanding the capsid structure of AAV viral vectors might facilitate the development of tissue-targeted AAV. Tropism can only be manipulated effectively when the sequences responsible for native tropism and sites amenable to the insertion of new epitopes are known. Recent work with AAV2 has shown some promise in identifying receptor recognition domains (33, 48), and a knowledge of the high-resolution structure of the AAV2 capsid has permitted these sites to be localized within a putative binding patch close to the threefold axis (49). In addition, several sites on the AAV2 capsid are amenable to the insertion of new epitopes (19, 29, 48). Notwithstanding these achievements, structural and functional studies of additional AAV serotypes have the potential to broaden the utility of AAV gene transfer vectors.

The pseudo-atomic model we have generated for AAV5 provides a basis for understanding the known differences between AAV5 and AAV2 regarding carbohydrate moiety recognition during infection. The basic patches on the sides of the AAV2 threefold axis mounds that are thought to control bind-

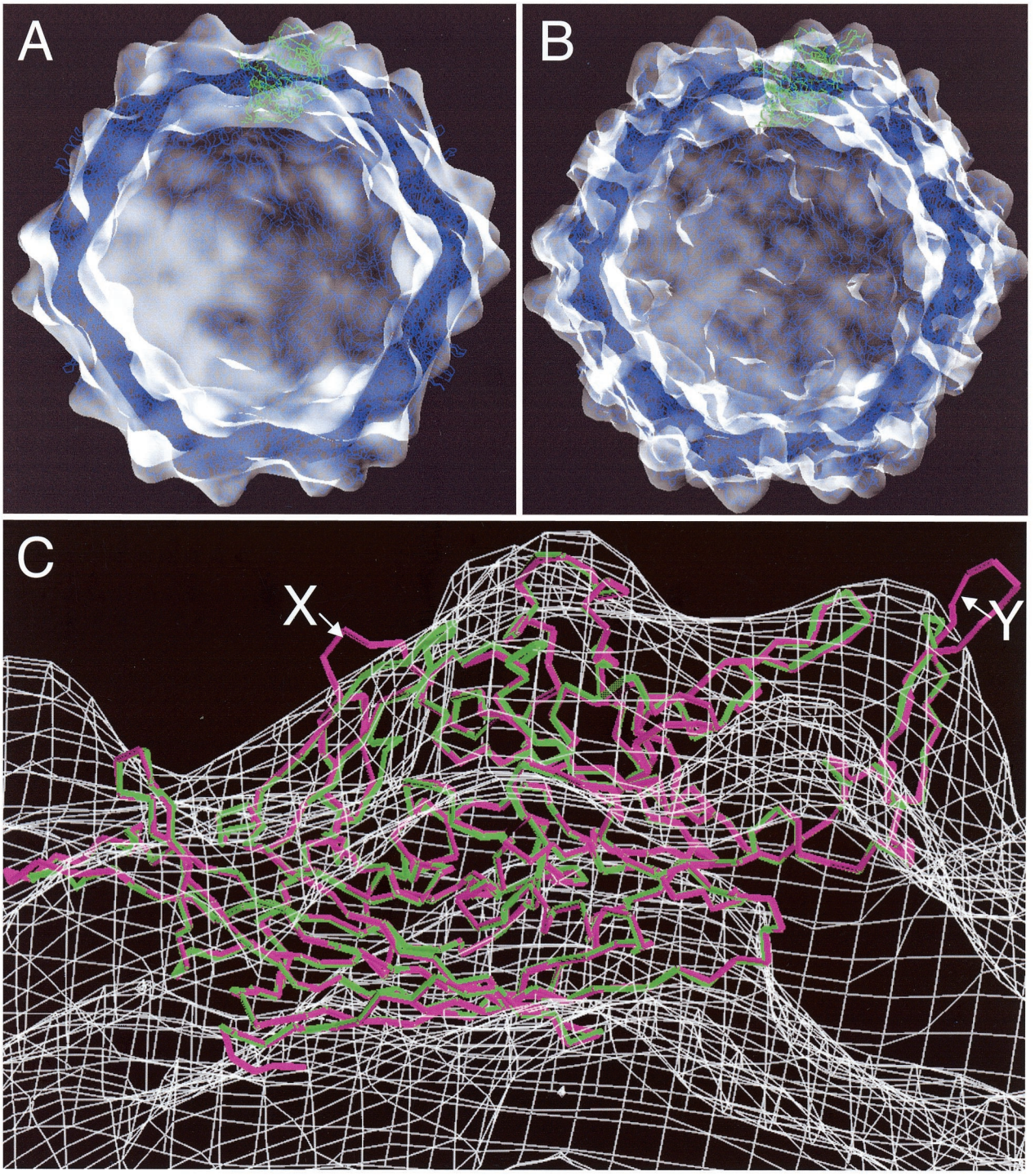

FIG. 6. Comparison of the AAV2-based model of AAV5 with the AAV5 reconstruction density. (A) Fit of AAV5 homology model (with a green Cα backbone of one VP3; all others are shown in blue) into cryo-EM density map (translucent gray envelope). The reconstruction is viewed from a direction slightly away from a twofold axis. (B) Same model as in panel A, but for a density map computed from a homology model of AAV5. (C) Close-up view of VP3 monomers (AAV2 is magenta and AAV5 is green) fit inside the reconstructed AAV5 density map (gray wire-frame). A single loop in the AAV5 model was repositioned to better fit the reconstruction density. AAV2 loops which extend outside the AAV5 reconstruction envelope are identified by arrows X and Y.

ing to heparan sulfate are missing from AAV5. In addition, the surface loops of the two serotypes differ at the tops of these mounds. These differences likely determine the precise nature of interactions during infection. However, since a specific sialic acid binding motif is yet to be identified, we are uncertain whether the same region of the capsid that controls heparan sulfate binding in AAV2 also controls sialic acid binding in AAV5. A comparison with CPV showed that the nature of the

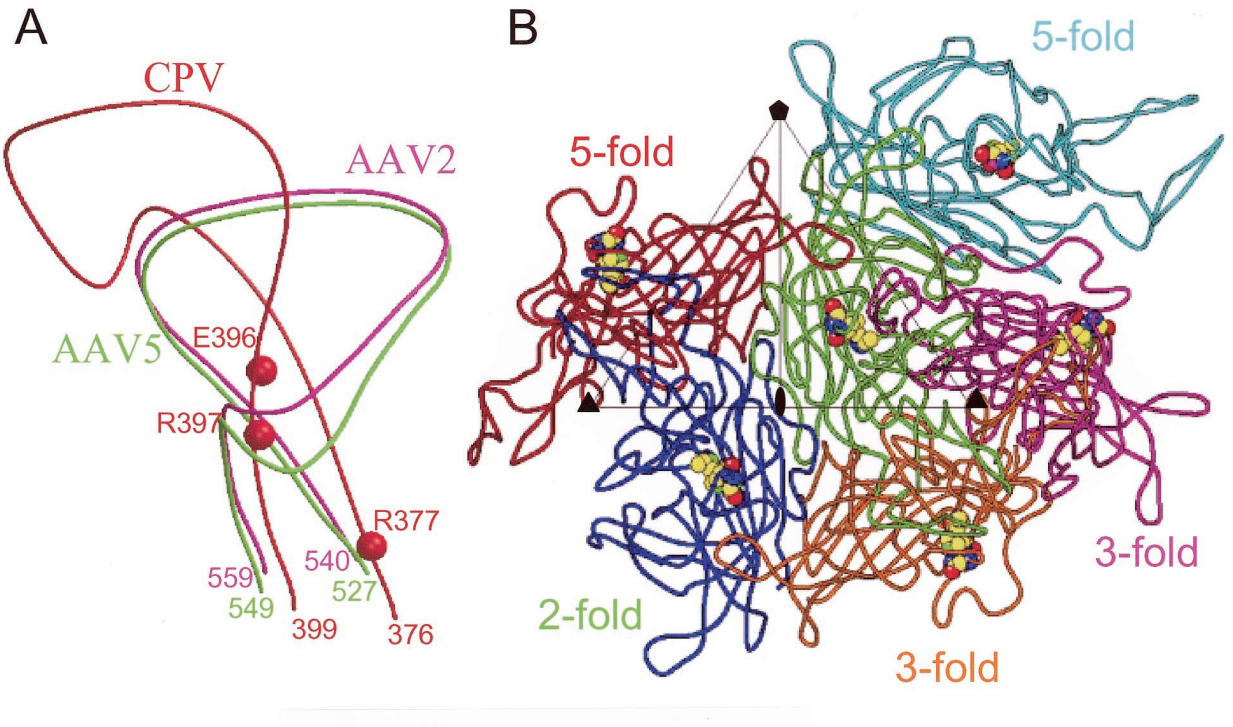

FIG. 7. Predicted sialic acid binding residues in AAV5. (A) Close-up view of corresponding surface loops in the AAV2 (magenta), AAV5 (green), and CPV (red) capsid subunits. Sialic acid binding residues in CPV are depicted as red spheres. Additional numbered residues (magenta, green, and red) represent the N and C termini of the depicted portions of the loops for each virus. (B) View towards viral capsid surface showing a VP3 reference monomer (green) plus one twofold (blue), two threefold (magenta and orange), and two fivefold (red and cyan) VP3 molecules. Residues were deduced by superimposing the AAV2-based model of AAV5 onto the CPV structure. Predicted sialic acid binding residues (528, 546, and 547) equivalent to those involved in CPV sialic acid binding are highlighted as space-filling structures.

AAV5 residues that are structurally equivalent to the CPV sialic acid binding residue and the surface loop configurations differ. Interestingly, AAV5 and AAV2 also differ slightly in the conformation of the loops containing these twofold axis-related residues. Knowledge of the specific site for sialic acid binding on AAV5 ought to provide a means for understanding how AAV5 contacts host cell surfaces. Models of AAV5 such as the one presented here can provide an essential starting point for these studies.

Humoral immunity is one of the most important processes that must be more deeply understood before transfer vectors become a viable option for gene therapy. A knowledge of antibody recognition domains across AAV serotypes could be important for designing vectors that evade neutralizing antibodies. This concept was recently highlighted by the work of Bloom and colleagues with ADV (8). Specifically, they found that neutralizing antibodies on surface-exposed residues of ADV could block receptor-mediated binding while enhancing antibody-mediated infection of macrophages. This explains the difficulty of developing effective vaccines for ADV (8). Concerning AAV vectors, neutralizing antibodies against AAV2 are known to be more prevalent in the general population than are neutralizing antibodies against AAV5 (22). Moreover, neutralizing antibodies in mice exposed to recombinant AAV2 are ineffective at preventing gene transfer by AAV5 (21). This observation is consistent with the fact that the AAV2 and AAV5 surface topologies differ at the loop surfaces associated with antibody interactions in AAV2. AAV2 and AAV5 show unprecedented similarities to ADV in terms of surface topology. It is possible that homologous AAV and ADV structural regions may also contribute to the antigenic phenotypes of these dependoviruses and that antibody binding may also interfere with primary host cell receptor recognition. The conformational epitope recognized by the A20 antibody in AAV2 lies on the wall between the two-, three-, and fivefold axes (49). This surface region is analogous to an epitope that is highly immunogenic in the ADV capsid. Thus, a combination of available data on AAV2 and ADV can be utilized with our structural data on the AAV5 capsid for probing its antigenic phenotype.

An understanding of structure-function relationships among dependent parvoviruses serves primarily to help with the development of gene transfer vectors. However, other members of the *Parvoviridae* family are important human and animal pathogens. For example, *Parvovirus* B19, a virus from the genus *Erythrovirus*, causes aplastic anemia, fifth disease, spontaneous abortion, and hydrops fetalis in humans (51). Likewise, RA-1 virus has been associated with rheumatoid arthritis.

Moreover, viruses from the genus *Parvovirus* are responsible for several animal diseases (e.g., ADV causes Aleutian mink disease and CPV causes canine parvovirus infection). While some of these viruses are difficult to grow and genetically manipulate, major efforts toward the production and purification of the AAVs improved our ability to manipulate, grow, and purify AAV (44). Hence, AAV may serve as a useful model for understanding a host of human and animal pathogens.

For this study, we determined the structure of AAV5 to 16-Å resolution by cryo-EM and image reconstruction and built a working pseudo-atomic model based on the structure of AAV2. AAV5 has features that are analogous to those of some parvovirus capsids, and it is remarkably similar to AAV2. This is consistent with previous observations of *Parvoviridae* with 50% or more sequence identity (3). However, surface loop regions differ, consistent with observed tropism and antigenic differences. AAV5 has some similarities to other sialic acid binding parvoviruses, but no specific surface feature appears to correlate with sialic acid binding. A more complete understanding of AAV5 capsid structure-function relationships will require more detailed characterizations of the AAV5 capsid structure. Our AAV2-based model of AAV5 provides a benchmark for designing genetic manipulations that can be used to better characterize the tropism and antigenic properties of AAV5.

ACKNOWLEDGMENTS

We thank Pary Weber, Tamara Nesselhauf, and Theresa Mayhew for excellent assistance and Michael Welsh for helpful discussions. We thank the University of Iowa In Vitro Models and Cell Culture Core (supported by the National Heart, Lung and Blood Institute, the Cystic Fibrosis Foundation, and the National Institute of Diabetes and Digestive and Kidney Diseases [DK54759]), the Gene Transfer Vector Core (supported by the Roy J. Carver Charitable Trust, the NHLBI, CFF, and NIDDK [DK54759]), and the University of Iowa Central Microscopy Research Facility.

This work is an equal collaboration between the laboratories of J.Z., J.A.C., M.A.-M., and T.S.B. This work was supported in part by the National Heart, Lung and Blood Institute and the Cystic Fibrosis Foundation, by NIH grant GM33050 to T.S.B., by NSF shared instrumentation grant BIR911291 to T.S.B. for the FEI CM200 FEG microscope, by a Purdue reinvestment grant to the Purdue Structural Biology group, and by an HHMI Biomedical Research Program pilot grant to M.A.-M.

REFERENCES

1. **Agbandje, M., S. Kajigaya, R. McKenna, N. S. Young, and M. G. Rossmann.** 1994. The structure of human parvovirus B19 at 8 Å resolution. Virology **203:**106–115.
2. **Agbandje, M., C. R. Parrish, and M. G. Rossmann.** 1995. The structure of parvoviruses. Semin. Virol. **6:**299–309.
3. **Agbandje-McKenna, M., A. L. Llamas-Saiz, F. Wang, P. Tattersall, and M. G. Rossmann.** 1998. Functional implications of the structure of the murine parvovirus, minute virus of mice. Structure **6:**1369–1381.
4. **Baker, T. S., N. H. Olson, and S. D. Fuller.** 1999. Adding the third dimension to virus life cycles: three-dimensional reconstruction of icosahedral viruses from cryo-electron micrographs. Microbiol. Mol. Biol. Rev. **63:**862–992.
5. **Barbis, D. P., S. F. Chang, and C. R. Parrish.** 1992. Mutations adjacent to the dimple of the canine parvovirus capsid structure affect sialic acid binding. Virology **191:**301–308.
6. **Beck, S. E., L. A. Jones, K. Chesnut, S. M. Walsh, T. C. Reynolds, B. J. Carter, F. B. Askin, T. R. Flotte, and W. B. Guggino.** 1999. Repeated delivery of adeno-associated virus vectors to the rabbit airway. J. Virol. **73:**9446–9455.
7. **Bewley, M. C., K. Springer, Y. B. Zhang, P. Freimuth, and J. M. Flanagan.** 1999. Structural analysis of the mechanism of adenovirus binding to its human cellular receptor, CAR. Science **286:**1579–1583.
8. **Bloom, M. E., S. M. Best, S. F. Hayes, R. D. Wells, J. B. Wolfinbarger, R. McKenna, and M. Agbandje-McKenna.** 2001. Identification of Aleutian mink disease parvovirus capsid sequences mediating antibody-dependent enhancement of infection, virus neutralization, and immune complex formation. J. Virol. **75:**11116–11127.
9. **Brunger, A. T., P. D. Adams, G. M. Clore, W. L. DeLano, P. Gros, R. W. Grosse-Kunstleve, J. S. Jiang, J. Kuszewski, M. Nilges, N. S. Pannu, R. J. Read, L. M. Rice, T. Simonson, and G. L. Warren.** 1998. Crystallography & NMR system: a new software suite for macromolecular structure determination. Acta Crystallogr. D **54:**905–921.
10. **Chipman, P. R., M. Agbandje-McKenna, S. Kajigaya, K. E. Brown, N. S. Young, T. S. Baker, and M. G. Rossmann.** 1996. Cryo-electron microscopy studies of empty capsids of human parvovirus B19 complexed with its cellular receptor. Proc. Natl. Acad. Sci. USA **93:**7502–7506.
11. **Collaborative Computational Project.** 1994. The CCP4 suite: programs for protein crystallography. Acta Crystallogr. D **50:**760–763.
12. **Cotmore, S. F., and P. Tattersall.** 1989. A genome-linked copy of the NS-1 polypeptide is located on the outside of infectious parvovirus particles. J. Virol. **63:**3902–3911.
13. **Duan, D., Y. Yue, Z. Yan, P. B. McCray, and J. F. Engelhardt.** 1998. Polarity influences the efficiency of recombinant adenoassociated virus infection in differentiated airway epithelia. Hum. Gene Ther. **9:**2761–2776.
14. **Fisher, K. J., K. Jooss, J. Alston, Y. Yang, S. E. Haecker, K. High, R. Pathak, S. E. Raper, and J. M. Wilson.** 1997. Recombinant adeno-associated virus for muscle directed gene therapy. Nat. Med. **3:**306–312.
15. **Flotte, T. R., S. A. Afione, R. Solow, M. L. Drumm, D. Markakis, W. B. Guggino, P. L. Zeitlin, and B. J. Carter.** 1993. Expression of the cystic fibrosis transmembrane conductance regulator from a novel adeno-associated virus promoter. J. Biol. Chem. **268:**3781–3790.
16. **Flotte, T. R., and B. J. Carter.** 1995. Adeno-associated virus vectors for gene therapy. Gene Ther. **2:**357–362.
17. **Fox, J. M., M. A. McCrackin Stevenson, and M. E. Bloom.** 1999. Replication of Aleutian mink disease parvovirus in vivo is influenced by residues in the VP2 protein. J. Virol. **73:**8713–8719.
18. **Gao, G., M. R. Alvira, S. Somanathan, Y. Lu, L. H. Vandengerghe, J. J. Rux, R. Calcedo, J. Sanmiguel, Z. Abbas, and J. M. Wilson.** 2003. Adeno-associated viruses undergo substantial evolution in primates during natural infections. Proc. Natl. Acad. Sci. USA **100:**6081–6086.
19. **Girod, A., M. Ried, C. Wobus, H. Lahm, K. Leike, J. Kleinschmidt, G. Deleage, and M. Hallek.** 1999. Genetic capsid modifications allow efficient re-targeting of adeno-associated virus type 2. Nat. Med. **5:**1052–1056.
20. **Guex, N., and M. C. Peitsch.** 1997. SWISS-MODEL and the Swiss-Pdb-Viewer: an environment for comparative protein modeling. Electrophoresis **18:**2714–2723.
21. **Halbert, C. L., E. A. Rutledge, J. M. Allen, D. W. Russell, and A. D. Miller.** 2000. Repeat transduction in the mouse lung by using adeno-associated virus vectors with different serotypes. J. Virol. **74:**1524–1532.
22. **Hildinger, M., A. Auricchio, G. Gao, L. Wang, N. Chirmule, and J. M. Wilson.** 2001. Hybrid vectors based on adeno-associated virus serotypes 2 and 5 for muscle-directed gene transfer. J. Virol. **75:**6199–6203.
23. **Hueffer, K., J. S. Parker, W. Weichert, R. E. Geisel, J. Y. Sgro, and C. R. Parrish.** 2003. The natural host range shift and subsequent evolution of canine parvovirus resulted from virus-specific binding to the canine transferrin receptor. J. Virol. **77:**1718–1726.
24. **Hughes, S. M., F. Moussavi-Harami, S. L. Sauter, and B. L. Davidson.** 2002. Viral-mediated gene transfer to mouse primary neural progenitor cells. Mol. Ther. **5:**16–24.
25. **Jones, T., J.-Y. Zou, S. W. Cowan, and M. Kjeldgaard.** 1991. Improved methods for building protein models in electron density maps and the location of errors in these models. Acta Crystallogr. A **47:**110–119.
26. **Kaludov, N., K. E. Brown, R. W. Walters, J. Zabner, and J. A. Chiorini.** 2001. Adeno-associated virus serotype 4 (AAV4) and AAV5 both require sialic acid binding for hemagglutination and efficient transduction but differ in sialic acid linkage specificity. J. Virol. **75:**6884–6893.
27. **Kay, M. A., C. S. Manno, M. V. Ragni, P. J. Larson, L. B. Couto, A. McClelland, B. Glader, A. J. Chew, S. J. Tai, R. W. Herzog, V. Arruda, F. Johnson, C. Scallan, E. Skarsgard, A. W. Flake, and K. A. High.** 2000. Evidence for gene transfer and expression of factor IX in haemophilia B patients treated with an AAV vector. Nat. Genet. **24:**257–261.
28. **Kleywegt, G. J., and T. A. Jones.** 1997. Model building and refinement practice. Methods Enzymol. **277:**208–230.
29. **Kronenberg, S., J. A. Kleinschmidt, and B. Bottcher.** 2001. Electron cryomicroscopy and image reconstruction of adeno-associated virus type 2 empty capsids. EMBO J. **2:**997–1002.
30. **Kurpad, C., P. Mukherjee, X. S. Wang, S. Ponnazhagan, L. Li, M. C. Yoder, and A. Srivastava.** 1999. Adeno-associated virus 2-mediated transduction and erythroid lineage-restricted expression from parvovirus B19p6 promoter in primary human hematopoietic progenitor cells. J. Hematother. Stem Cell Res. **8:**585–592.
31. **McKenna, R., N. H. Olson, P. R. Chipman, T. S. Baker, T. F. Booth, J. Christensen, B. Aasted, J. M. Fox, M. E. Bloom, J. B. Wolfinbarger, and M. Agbandje-McKenna.** 1999. Three-dimensional structure of Aleutian

mink disease parvovirus: implications for disease pathogenicity. J. Virol. **73:**6882–6891.
32. **Muzyczka, N.** 1992. Use of adeno-associated virus as a general transduction vector for mammalian cells. Curr. Top. Microbiol. Immunol. **158:**97–129.
33. **Opie, S. R., J. K. H. J. Warrington, M. Agbandje-McKenna, S. Zolotukhin, and N. Muzyczka.** 2003. Identification of amino acid residues in the capsid proteins of adeno-associated virus type 2 that contribute to heparan sulfate proteoglycan binding. J. Virol. **77:**6995–7006.
34. **Parker, J. S., W. J. Murphy, D. Wang, S. J. O'Brien, and C. R. Parrish.** 2001. Canine and feline parvoviruses can use human or feline transferrin receptors to bind, enter, and infect cells. J. Virol. **75:**3896–3902.
35. **Peitsch, M. C.** 1996. ProMod and Swiss-Model: Internet-based tools for automated comparative protein modelling. Biochem. Soc. Trans. **24:**274–279.
36. **Peitsch, M. C.** 1995. Protein modeling by e-mail. Bio/Technology **13:**658–660.
37. **Samulski, R. J., K. I. Berns, M. Tan, and N. Muzyczka.** 1982. Cloning of adeno-associated virus into pBR322: rescue of intact virus from the recombinant plasmid in human cells. Proc. Natl. Acad. Sci. USA **79:**2077–2081.
38. **Snyder, R. O., C. H. Miao, G. A. Patijn, S. K. Spratt, O. Danos, D. Nagy, A. M. Gown, B. Winther, L. Meuse, L. K. Cohen, A. R. Thompson, and M. A. Kay.** 1997. Persistent and therapeutic concentrations of human factor IX in mice after hepatic gene transfer of recombinant AAV vectors. Nat. Genet. **16:**270–276.
39. **Teramoto, S., J. S. Bartlett, D. McCarty, X. Xiao, R. J. Samulski, and R. C. Boucher.** 1998. Factors influencing adeno-associated virus-mediated gene transfer to human cystic fibrosis airway epithelial cells: comparison with adenovirus vectors. J. Virol. **72:**8904–8912.
40. **Thacker, T. C., and F. B. Johnson.** 1998. Binding of bovine parvovirus to erythrocyte membrane sialylglycoproteins. J. Gen. Virol. **79:**2163–2169.
41. **Thompson, J. D., D. G. Higgins, and T. J. Gibson.** 1994. CLUSTAL W: improving the sensitivity of progressive multiple sequence alignment through sequence weighting, position-specific gap penalties and weight matrix choice. Nucleic Acids Res. **22:**4673–4680.
42. **Tresnan, D. B., L. Southard, W. Weichert, J. Y. Sgro, and C. R. Parrish.** 1995. Analysis of the cell and erythrocyte binding activities of the dimple and canyon regions of the canine parvovirus capsid. Virology **211:**123–132.
43. **Tsao, J., M. S. Chapman, M. Agbandje, W. Keller, K. Smith, H. Wu, M. Luo, T. J. Smith, M. G. Rossmann, R. W. Compans, et al.** 1991. The three-dimensional structure of canine parvovirus and its functional implications. Science **251:**1456–1464.
44. **Urabe, M., C. Ding, and R. M. Kotin.** 2002. Insect cells as a factory to produce adeno-associated virus type 2 vectors. Hum. Gene Ther. **13:**1935–1943.
45. **Wagner, J. A., T. Reynolds, M. L. Moran, R. B. Moss, J. J. Wine, T. R. Flotte, and P. Gardner.** 1998. Efficient and persistent gene transfer of AAV-CFTR in maxillary sinus. Lancet **351:**1702–1703.
46. **Walters, R. W., S. M. Yi, S. Keshavjee, K. E. Brown, M. J. Welsh, J. A. Chiorini, and J. Zabner.** 2001. Binding of adeno-associated virus type 5 to 2,3-linked sialic acid is required for gene transfer. J. Biol. Chem. **276:**20610–20616.
47. **Wikoff, W. R., G. Wang, C. R. Parrish, R. H. Cheng, M. L. Strassheim, T. S. Baker, and M. G. Rossmann.** 1994. The structure of a neutralized virus: canine parvovirus complexed with neutralizing antibody fragment. Structure **2:**595–607.
48. **Wu, P., W. Xiao, T. Conlon, J. Hughes, M. Agbandje-McKenna, T. Ferkol, T. R. Flotte, and N. Muzyczka.** 2000. Mutational analysis of the adeno-associated virus type 2 (AAV2) capsid gene and construction of AAV2 vectors with altered tropism. J. Virol. **74:**8635–8647.
49. **Xie, Q., W. Bu, S. Bhatia, J. Hare, T. Somasundaram, A. Azzi, and M. S. Chapman.** 2002. The atomic structure of adeno-associated virus (AAV-2), a vector for human gene therapy. Proc. Natl. Acad. Sci. USA **99:**10405–10410.
50. **Yang, G. S., M. Schmidt, Z. Yan, J. D. Lindbloom, T. C. Harding, B. A. Donahue, J. F. Engelhardt, R. Kotin, and B. L. Davidson.** 2002. Virus-mediated transduction of murine retina with adeno-associated virus: effects of viral capsid and genome size. J. Virol. **76:**7651–7660.
51. **Young, N. S.** 1996. Parvoviruses, p. 2199–2221. *In* B. N. Fields, D. M. Knipe, and P. M. Howley (ed.), Fields virology, 3rd ed., vol. 2. Lippincott Williams & Wilkins, Philadelphia, Pa.
52. **Zabner, J., M. Seiler, R. Walters, R. M. Kotin, W. Fulgeras, B. L. Davidson, and J. A. Chiorini.** 2000. Adeno-associated virus type 5 (AAV5) but not AAV2 binds to the apical surfaces of airway epithelia and facilitates gene transfer. J. Virol. **74:**3852–3858.
53. **Zabner, J., B. G. Zeiher, E. Friedman, and M. J. Welsh.** 1996. Adenovirus-mediated gene transfer to ciliated airway epithelia requires prolonged incubation time. J. Virol. **70:**6994–7003.